Dynamic Droop Setting of Smart Inverters in Active Distribution Grid using Neural Networks

Aashutosh Neupane and Sumit Paudyal
Florida International University, Miami, USA
Emails: {aneup003, spaudyal}@fiu.edu

***Abstract*—Increasing penetration of Smart Inverters (SIs) will shift the voltage control functionalities to the grid edge. With the advanced control mechanism and capabilities of SIs to dynamically adjust Volt-Watt and Volt-VAr droops, better and granular voltage regulation can be achieved on distribution feeders. In this context, this paper discusses the application of Neural Networks (NNs) through which effective setting of SIs' droops could be obtained leading to better voltage regulation on distribution feeders. Case studies on the IEEE 123-node feeder shows effective voltage regulation from SIs with droop settings obtained from the NNs.**

***Index Terms*—Neural Networks, Photovoltaics, Smart Inverters, Voltage Control, Volt-VAr**

I. Introduction

The advancements of control technologies at distribution level has opened new opportunities for Distribution System Operators (DSOs) for better managing and operating active distribution networks [1]. The global adoption of distributed energy resources (DERs) is accelerating, providing benefits such as enhanced flexibility in grid operations. The photovoltaic (PV) is the most rapidly expanding energy source which had the most prominent growth at the distribution level over the past decade. However, distribution grid posses limited capacity to accommodate DERs. The substantial increase in the generation of the PV power may lead to adverse effects, including backward flow of power and voltage issues. Control of voltage in distribution grid is a crucial task handled through distribution management system (DMS) that is designed to maintain local service voltages within the limit specified by American National Standards Institute (ANSI). The updated IEEE-1547 standard permits DERs to assist with voltage regulation by utilizing droop based control for active and reactive power at the point of common coupling (PCC). IEEE-1547 plays a crucial role in the standardizing of the operational capabilities of the modern DERs, facilitating their integration into the power grid as valuable assets. Unlike conventional inverters, Smart Inverters (SIs) possess advanced self-governing features, allowing them to operate seamlessly across a broad range of frequency and voltage disturbances without disconnection during overvoltage incidents. Volt-VAr Optimization (VVO) based on Distribution Grid Optimal Power Flow (DOPF) can deliver viable solutions across the entire network by taking into account the complete topology of the network, time-based recordings, and the Volt-VAr droop characteristics of SIs, as well as reducing the effects of the variability in PV generation [1]. The control mechanism can also autonomously regulate the reactive power output of SI within an established voltage range, in accordance with the droop functions defined in IEEE 1547 [2]. Specifically, the utilization of the SI local droop in VVO functionality provides feasible solutions to mitigate voltage issues and maximize the hosting capacity of PV, especially with significant penetration of PV resources in the distribution grid.

In recent days, Neural Network (NN) based approaches has been widely used in development of voltage control models and Volt-VAr control in distribution grid. The application of NN in such control models relies on accurate information of grid parameters, which can be challenging to obtain in real-life scenarios. NN, especially Long Short-Term Memory (LSTM), appears promising for predicting the system states in the distribution networks [3]. Forehand knowledge of the voltage at distribution grid network can help the utility service providers to mitigate the overvoltage condition and ensure the reliable operations of the grid. This study outlines to show the performance of LSTM in predicting the droop settings of SIs in the distribution network. The dynamically adjusted droop can help in managing the voltage of the power grid more effectively.

The remainder of the paper is organized as follows. Section II outlines the math modeling of Q(V), Section III provides background information, Section IV discusses the methodology, and Section V presents the Case Study and Results. Finally, Section VI summarizes the conclusion and future work.

II. Math Modeling

A. Photovoltaic (PV) Inverter Control

PV system is comprised of solar panels which absorbs sunlight and converts it into a direct current (dc), which is then transformed into an alternating current (ac) using an inverter. The term SI in this study refers to a PV-based inverter that is connected to the grid at the PCC. This inverter operates in two quadrants, allowing it to both provide and absorb reactive power as needed. The PV system operates with a power factor that is leading and behaves like a capacitive generator in the injection mode. It behaves like an inductive generator, drawing the reactive power from the grid with a power factor that is lagging during the absorption mode, as depicted in Fig. 1. The reactive power the SI can supply is determined by its apparent power rating, which can be expressed mathematically as follows:

$$\sqrt{\left(p_i^G\right)^2 + \left(q_i^G\right)^2} \leq s_i^G, \quad \forall i \in \mathcal{B}^{\mathcal{G}} \tag{1}$$

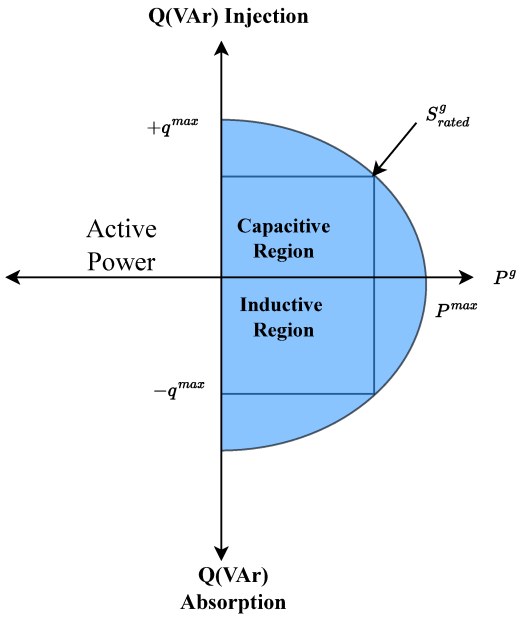

Fig. 1: Operating zones of PV Inverter.

where ${p_i}^G$ and ${q_i}^G$ denote active and reactive power outputs of PV. ${s_i}^G$ denotes the apparent power rating. $\mathcal{B}^{\mathcal{G}}$ represents the collection of nodes connected to PV, and i represents the index of the node to which the SI is connected to.

The active and reactive power output capabilities are limited by the following constraints,

$$0 \leq p_i^G \leq p_i^{G,\max}, \quad \forall i \in \mathcal{B}^{\mathcal{G}} \tag{2}$$

$$-q_i^{G,\max} \leq q_i^G \leq q_i^{G,\max}, \quad \forall i \in \mathcal{B}^{\mathcal{G}} \tag{3}$$

where $p_i^{G,\max}$ is proportional to the solar irradiation. The net active and reactive power injections at node i are defined as $p_i = p_i^G - p_i^C$ and $q_i = q_i^G - q_i^C$, where p_i^C (q_i^C) indicates the active (reactive) power consumption at node i.

B. Volt-VAr Droop Function of the Smart Inverters

The voltage at the PCC is defined by the Volt-VAr function of SIs which determines the reactive power output from the SIs, represented by $\boldsymbol{Q(V)}$, commonly referred to as Volt-VAr curve or droop. The piecewise linear relationship between reactive power generation and the voltage at PCC for $\boldsymbol{Q(V)}$ droop configuration is illustrated in Fig. 2. There is no absorption or injection of reactive power, in the voltage range of $(V_{i,3}, V_{i,4}]$, referred to as the deadband. In the range of $(V_{i,2}, V_{i,3}]$ the voltage value decreases, and the SI operates in the modulation of the reactive power generation mode, and smaller voltage values within $[V_i^l, V_{i,2})$ pushes the SI into capacitive saturation zone. Similarly, in the interval $(V_{i,4}, V_{i,5}]$ the SI operates in the inductive mode along the slope and the SI continues to operate in inductive saturation in the range of $(V_{i,5}, V_i^u]$. On the basis of these breakpoints, the accessible voltage operating range is divided into several segments that determine the control actions of the SIs.

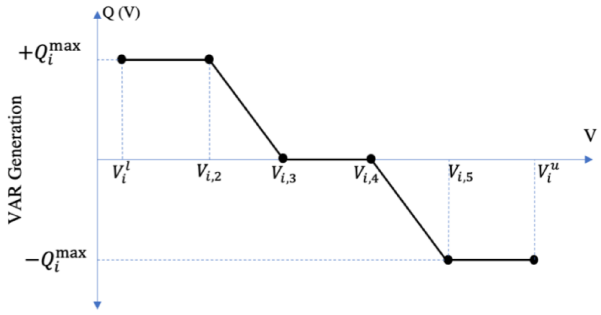

Fig. 2: Smart Inverter Q(V) droop curve [2].

The piecewise function of the Q(V) droop curve can be expressed mathematically as,

$$Q_i\left(V_i\right) = \begin{cases} +Q_i^{\max}, & V_i^l \leq V_i \leq V_{i,2} \\ \frac{-Q_i^{\max}}{V_{i,3}-V_{i,2}} V_i + \frac{Q_i^{\max} V_{i,3}}{V_{i,3}-V_{i,2}}, & V_{i,2} < V_i \leq V_{i,3} \\ 0, & V_{i,3} < V_i \leq V_{i,4} \\ \frac{-Q_i^{\max}}{V_{i,5}-V_{i,4}} V_i + \frac{Q_i^{\max} V_{i,4}}{V_{i,5}-V_{i,4}}, & V_{i,4} < V_i \leq V_{i,5} \\ -Q_i^{\max}, & V_{i,5} < V_i \leq V_i^u \end{cases} \tag{4}$$

where V_i represents the voltage at node i, with minimum and maximum limits indicated as V_i^l and V_i^u, respectively. The interval from $V_{i,2}$ to $V_{i,5}$ represents the voltage thresholds for V_i and Q_i^{max} indicates the maximum rating of reactive power of SI.

III. Background

A. Long Short Term Memory

LSTM, which is a variant of the Recurrent Neural Network (RNN), excels at extracting information from the previous time step [4]. LSTM was introduced by Hochreiter and Schmidhuber to address challenges associated with long-term predictions. The typical structure of the LSTM cell comprises of input gate, forget gate, and output gate [5], which is illustrated in Fig. 3.

The input component of the LSTM consists of three elements: the input x_t at time t, the memory block with state C_{t-1} at previous time step $t-1$ as well as the hidden layer state of the cell h_t-1. The output element consists of memory block denoted by C_t at time t and the hidden layer with state of h_t at time t. The input x_t is constrained by the sigmoid activation function within the range of [0,1] to allow for the regulation of variables and facilitate the influence of x_t on C_t. The forget gate's function is to selectively disregard the information from the previous time step by utilizing the memory block C_{t-1} to manage C_t. The output gate evaluates the extent to which C_t impacts h_t to generate the output and regulate the variables. The mathematical steps can be represented as,

$$\boldsymbol{i}_t = \sigma\left(\boldsymbol{W}_{it}\boldsymbol{x}_t + \boldsymbol{W}_{ih}\boldsymbol{h}_{t-1} + b_i\right), \tag{5}$$

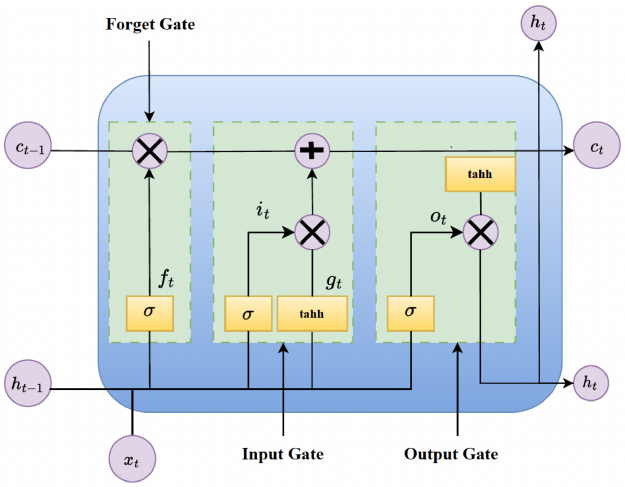

Fig. 3: Architecture of LSTM Unit.

$$\boldsymbol{f}_t = \sigma\left(\boldsymbol{W}_{fx}\boldsymbol{x}_t + \boldsymbol{W}_{fh}\boldsymbol{h}_{t-1} + b_f\right), \tag{6}$$

$$\boldsymbol{o}_t = \sigma\left(\boldsymbol{W}_{ox}\boldsymbol{x}_t + \boldsymbol{W}_{oh}\boldsymbol{h}_{t-1} + b_o\right), \tag{7}$$

where sigmoid is the activation function denoted by σ, the computed output of forget gate, input gate, and output gate is given by f_t ,i_t and o_t, respectively. The matrices W_{fx}, W_{it}, W_{ox} and the bias term b_f, b_i, b_o correspond to the weights and biases associated with each LSTM gate. The final output for the memory block at time t is influenced by the cell state and output gate [6], and is calculated as,

$$\boldsymbol{C}'_t = \tanh\left(\boldsymbol{W}_c \cdot \boldsymbol{h}_{t-1} + \boldsymbol{W}_f \cdot \boldsymbol{x}_t + b_c\right), \tag{8}$$

$$\boldsymbol{C}_t = \boldsymbol{f}_t \,.\boldsymbol{C}_{t-1} + \boldsymbol{i}_t \,.\boldsymbol{C}'_t, \tag{9}$$

$$\boldsymbol{h}_t = \boldsymbol{o}_t.\ tanh(\boldsymbol{C}_t), \tag{10}$$

where the activation function is $tanh()$ and $\boldsymbol{C}'_t$ represents state input of LSTM cell at instant t. The bias term and input layer state weight matrix corresponds to b_c and $\boldsymbol{W_c}$ respectively. The "." operator represents element-wise multiplication.

B. Performance Evaluation of LSTM

The effectiveness of the LSTM model to predict the voltage across different temporal contexts was assessed by computing the Root Mean Squared Error (RMSE) between the predicted and true voltage values. RMSE is widely employed metric for quantifying the error between true and predicted values and can be expressed mathematically as,

$$RMSE = \sqrt{\frac{1}{N}\sum_{k=1}^{N}\left(f\left(x_k\right) - y_k\right)^2} \tag{11}$$

Here, k, N represents the sample index and total number of data sample respectively. The forecasted value of k^{th} data sample is given by $f(x_k)$ and y_k denotes the true value of the k^{th} sample of the dataset. Models with the lower RMSE indicates improved accuracy since RMSE offers numerical assessment of model's prediction accuracy.

IV. Methodology

The study is divided into two parts. First, the voltage measurements were collected from 13 nodes of the IEEE 123-node test feeder. Then, the second stage involves utilizing the NN to forecast the droop settings for future time using LSTM.

A. Simulation Setup

The Python programming acts as the platform for extracting data from the IEEE test feeder with PV systems, each connected to SIs with droop control that complies with the IEEE 1547 (see Fig. 4). Voltage conditions within the environment are determined at specific instances through the integration of OpenDSS software with Python, facilitated by the COM interface. This integration enables smooth control of the OpenDSS software from Python, streamlining the data retrieval process. The distribution feeder designed in the OpenDSS is 123-node test feeder with 7 PVs of 600kW each as shown in the Fig. 5. The OpenDSS solves the network for the given parameters and the resulting voltage solution is extracted through the interface of Python and OpenDSS. The data is collected with varying droop setpoint of the SIs, irradiation, and load shape curve in time series format. The droop settings were identical for all 7 SIs, and were varied every 30 minutes for 17,520 times, which is equivalent to 365 days with 30-min time resolution. The collected 17,520 inputs were the data used in the training, validation, and testing of the LSTM NN in the split ratio of 80%, 10%, and 10%, respectively. The LSTM model used for this case study is shown in Fig. 7. Thirty two input parameters are fed to NN and the network predicted two outputs. The input parameters were nodal voltage V (in p.u.) and droop setpoint of SIs. The outputs were the droop set points of the SIs. The location of buses where the voltage is measured in the IEEE 123-node test feeder in OpenDSS as input data for NN model is shown in Fig. 6.

1) Architecture of LSTM: In this study, multi input LSTM network is proposed for predicting the volt-VAr droop settings of the SIs. A total of 30 voltage values from different buses and 2 droop setpoint values were given as input to the LSTM, making it a total of 32 inputs to the model, which predicts 2 output droopset point values. LSTM NN in our study has

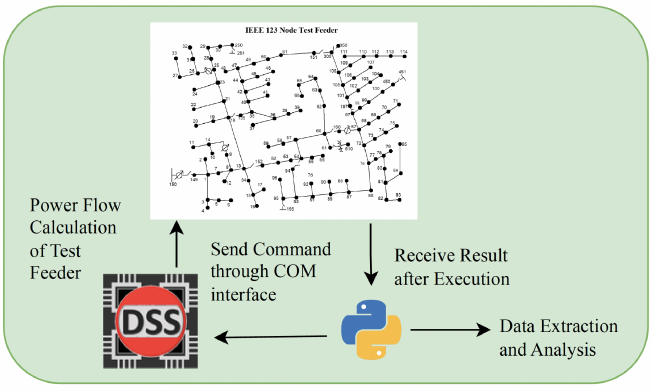

Fig. 4: Schematic representing Data Extraction Method.

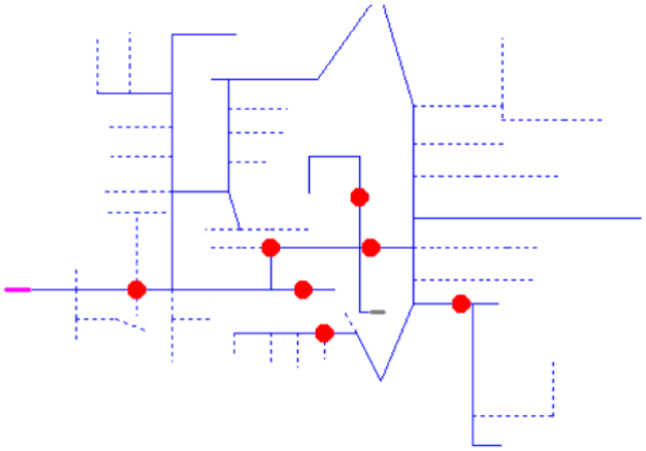

Fig. 5: Location of PV Units in IEEE 123-Node Test Feeder.

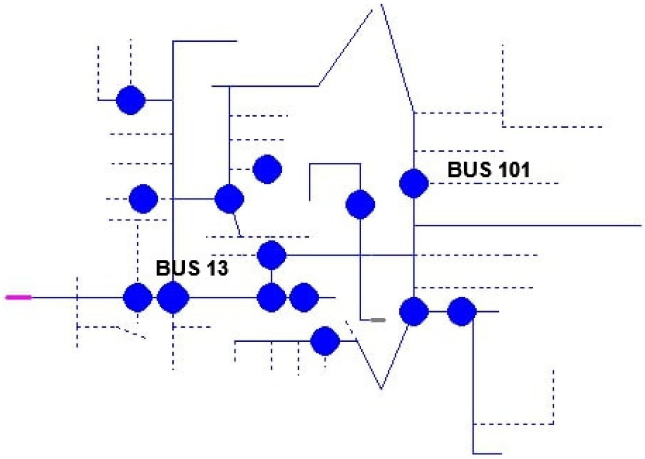

Fig. 6: Location of Monitoring Units in IEEE 123-Node Test Feeder.

feedback connections, which enhances its ability to process data sequences and predict time-series data. It consists of four number of LSTM layer and single dense layers at the end. Inorder to improve the training process, four dropout layer one after each LSTM layer has been added. The architecture of the LSTM NN model is shown in Fig. 7.

The LSTM input voltage data were subjected to pre-processing normalization, scaled to a range of 0 to 1 by employing the min-max normalization ($\boldsymbol{F}_{norm}$) equation in (12), where $\boldsymbol{F}$ denotes the true value of the feature being normalized, $\boldsymbol{F}_{max}$ represents the maximum value of the feature $\boldsymbol{F}$ in the dataset and $\boldsymbol{F}_{min}$ represents the minimum value of the feature $\boldsymbol{F}$ in the dataset. This normalization step is essential to make the input data in a uniform scale, and enhance the performance of the NN model.

$$\boldsymbol{F}_{norm} = (\boldsymbol{F} - \boldsymbol{F}_{min})/(\boldsymbol{F}_{max} - \boldsymbol{F}_{min}) \tag{12}$$

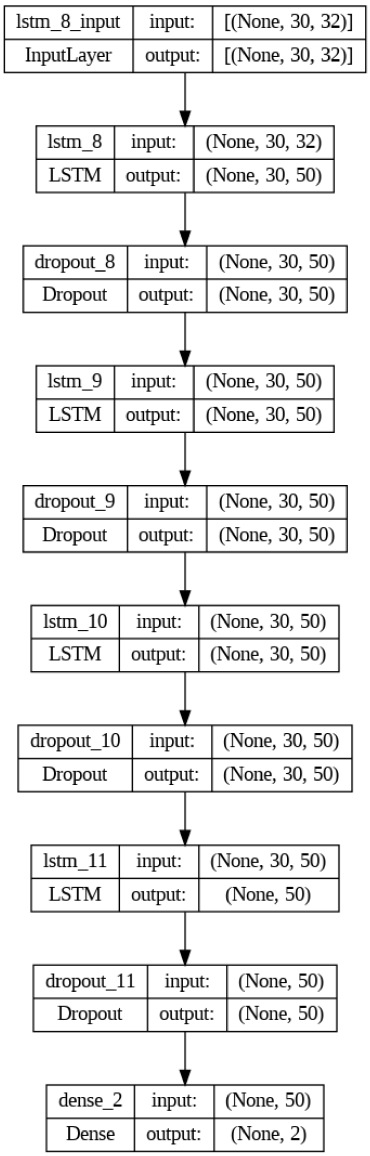

Fig. 7: Architecture of LSTM.

V. Case Study and Results

For the evaluation of overall performance of the obtained droop settings of SIs, the voltage at bus-13 and bus-101 of the IEEE 123-node test feeder is shown. Bus-13 is closer to the substation, while bus-101 is away from the substation; however, both buses lie nearby the node where SIs are connected to (please refer to Fig. 5 and Fig. 6). The obtained droop setting are dynamic that changes every 30 minutes, and two time series voltage plot for 2 hours time on Phase a at bus-13 and bus-101 are shown in Fig. 8 and Fig. 9. The droop time-frame selected has droop setpoints predicted by NN at $t-2$, $t-1$, t, $t+1$. The droops obtained from NN are used in OpenDSS Python Interface under the similar setting of irradiation, load shape to evaluate whether the predicted droop setpoints result in satisfactory output voltages. It can be inferred from the plot that the voltages in the bus are well within the range for different predicted droop settings, different scenarios of

load shapes and solar irradiation. The predicted droop setting of volt-VAr seems to maintain the voltage most of the time except some instances as shown by Vmax (max voltage limit) in Fig. 9. An example output volt-VAr droop value predicted from the proposed NN is shown in Fig. 10. The predicted droop setting obtained from NN confirms the droop setting recommended in the IEEE 1547.

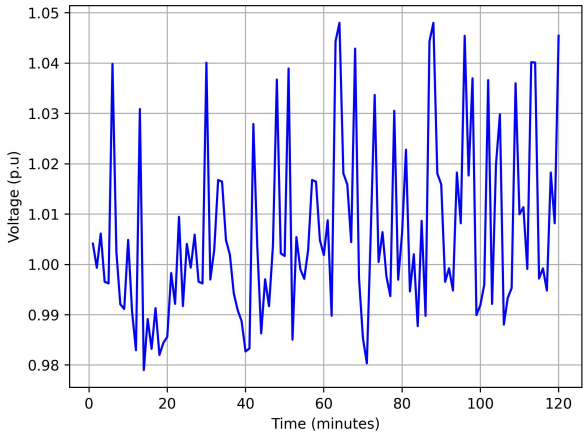

Fig. 8: Voltage vs. time plot with predicted Droop Setpoints at bus-13.

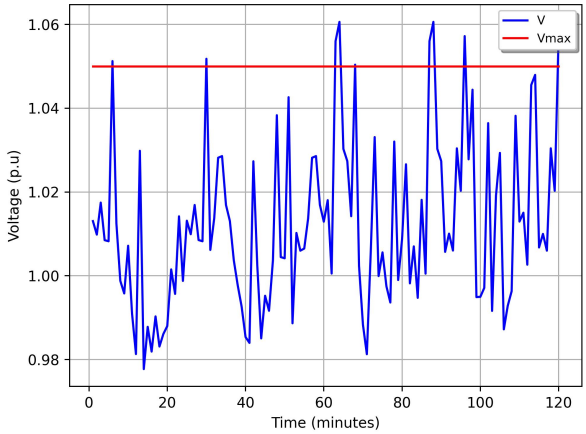

Fig. 9: Voltage vs. time plot with predicted Droop Setpoints at bus-101.

It can be observed from Fig. 11 and Fig. 12, the μ distribution of voltage measurement at bus-13 and bus-101 lies around 1.02 p.u which can be interpreted as in the normal range. This underlying data distribution also indicates that dynamic droop setting mechanics is effective in maintaining the system voltage on varying grid conditions.

Fig. 13 shows the progress of the RMSE loss against the epoch number for NN model. Figure shows that RMSE loss decreases for training and validation data set with final RMSE loss value of 0.0141 and 0.0077, respectively. This performance of the RMSE loss on training and validation data ascertains that LSTM NN is good in predicting the droops of SIs. Furthermore, the accuracy of the model was validated using the RMSE as the metric for the first 2 hours of predicted voltage data at bus-13 and bus-101 against the actual voltage data, and was found to have RMSE of 0.024677 and 0.02497, respectively. This low value of RMSE shows our approach of using NN for droop prediction for effective voltage regulation of active distribution network.

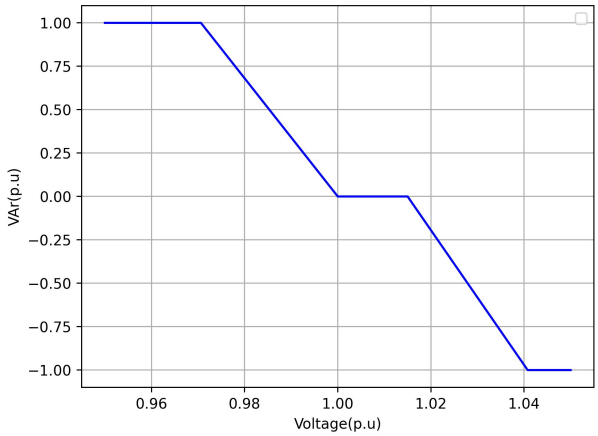

Fig. 10: A Typical Volt-VAr curve obtained with droop values predicted by NN.

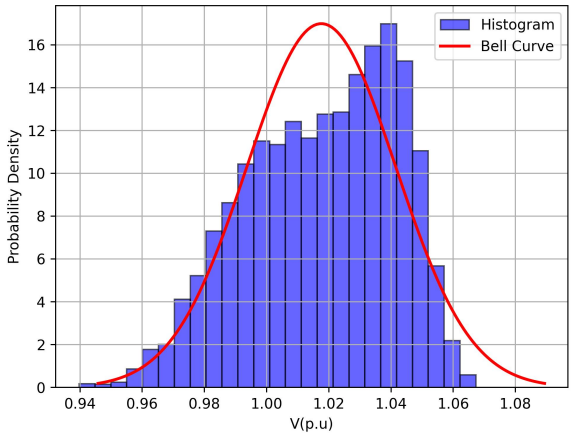

Fig. 11: Distribution of voltage at bus-13.

VI. Conclusions and Future Work

Accurate and dynamic droop settings enable effective voltage regulation and reactive power support in the power grid. The SIs plays a critical role for supporting and enhancing grid capability as well as enabling the integration of higher level of DER in the grid. The prediction of the set point of the Volt-VAr curve has been observed in this work using the LSTM Network through the use of historical time series voltage measurements. Two observation has been presented,

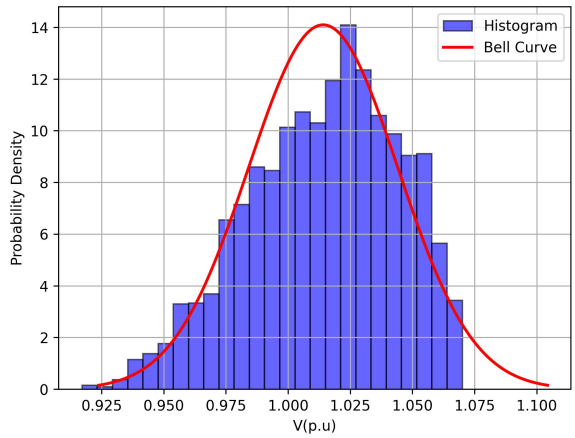

Fig. 12: Distribution of voltage at bus-101.

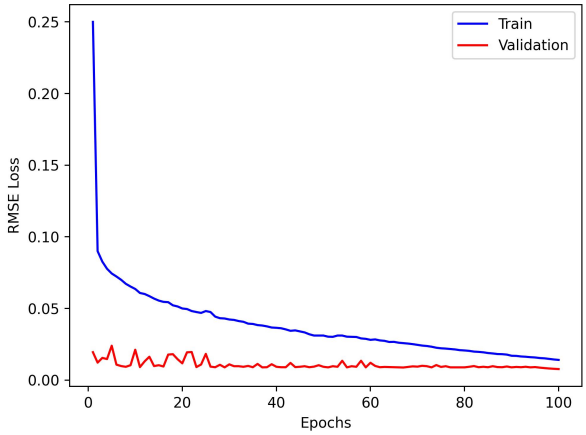

Fig. 13: RMSE Loss vs. the epoch number.

proving the efficacy of the predicted droop values using the NN. From the observed voltage, a normal distribution curve is presented which gives underlying voltage data distribution based on the location of the bus in the test feeder when the Volt-VAr droop setting is dynamically varied. This paper has laid the foundation for the application of the prediction of the droop control, to ensure effective voltage and reactive power control on distribution feeders. However, other various features such as optimal droop settings that follow IEEE 1547 guidelines without any undervoltage or overvoltage issue needs to be carried out in the future studies.

REFERENCES

[1] A. Savasci, A. Inaolaji, and S. Paudyal, "Distribution Grid Optimal Power Flow with Adaptive Volt-VAr Droop of Smart Inverters," in *Proc. IEEE Industry Applications Society Annual Meeting (IAS)*, 2021, pp. 1–8.

[2] "IEEE Standard for Interconnection and Interoperability of Distributed Energy Resources with Associated Electric Power Systems Interfaces," *IEEE Std 1547-2018 (Revision of IEEE Std 1547-2003)*, pp. 1–138, 2018.

[3] R. Henry and R. K. Gupta, "Measurement - Based/Model-Less Estimation of Voltage Sensitivity Coefficients by Feedforward and LSTM Neural Networks in Power Distribution Grids," in *Proc. IEEE Texas Power and Energy Conference (TPEC)*, 2024, pp. 1–6.

[4] P. Mali and S. Paudyal, "Neural Network-Based Load-Frequency Control in Power Grids," in *Proc. 2023 North American Power Symposium (NAPS)*, 2023, pp. 1–6.

[5] M. R. Hossain, S. Paudyal, and T. Vu, "Recurrent Neural Networks for Solving Photovoltaic System Dynamics," in *Proc. IEEE PES Innovative Smart Grid Technologies Latin America (ISGT-LA)*, 2023, pp. 260–264.

[6] D. Liu, Y. Wang, Y. Zhang, Y. Wang, Q. Zhu, and B. Zhang, "Temperature Prediction of Transformer High-Voltage Bushing Based on PSO-LSTM," in *Proc. IEEE Conference on Electrical Insulation and Dielectric Phenomena (CEIDP)*, 2022, pp. 91–94.